The International Journal of Advanced Manufacturing Technology (2018) 96:2791–2801
https://doi.org/10.1007/s00170-018-1728-0

ORIGINAL ARTICLE

Defect detection in selective laser melting technology by acoustic signals with deep belief networks

Dongsen Ye[1] · Geok Soon Hong[2] · Yingjie Zhang[2] · Kunpeng Zhu[3] · Jerry Ying Hsi Fuh[2]

Received: 5 September 2017 / Accepted: 6 February 2018 / Published online: 24 February 2018

Abstract
Selective laser melting (SLM) is one of the most important and successfully additive manufacturing processes in 3D metal printing technologies. Critical quality issues such as porosity, surface roughness, crack, and delamination continue to present challenges within SLM-manufactured parts. Monitoring and in-process defect diagnosis are the key to improving the final part quality. Currently, it greatly hinders the adaptability and the development within the defect detection system since the setup restricts the vision and photo diode applications in the SLM process monitoring. Additionally, defect detection with traditional classification approaches makes the system rather complex due to introducing a series of steps. To meet these needs, this study proposes a novel method for the defect detection within the SLM parts. The setup was flexibly conducted using a microphone, and the defect detection was obtained by the framework of deep belief network (DBN). It is implemented by a simplified classification structure without signal preprocessing and feature extraction. The experimental results showed that the utilization of acoustic signals was workable for quality monitoring, and the DBN approach could reach high defect detection rate among five melted states without signal preprocessing.

Keywords Additive manufacturing · Deep belief networks · Fast Fourier transform · Defect detection

1 Introduction

Selective laser melting (SLM) technology is one of the most promising processes of metal-based additive manufacturing (AM) technology [1]. It can directly achieve components with long fatigue life, fine surface finish, and high density from a metal powder bed layer by layer. However, critical product quality issues such as irregular porosity, crack, and delamination continue to present challenges among SLM-manufactured parts [2]. Feedback controls subsequent to the quality monitoring of the SLM process could generally minimize this variability for improving the quality of metal parts. Nevertheless, it is impeded by lacking process monitoring techniques. Therefore, it is necessary to develop in situ process measurement methods to facilitate the monitoring of the SLM process.

The primary quality issues are balling, warp, crack, and delamination in components from the SLM process. The balling effect is generally caused by insufficient wetting, over wetting, or sparking [3]. It will result in the increase of pores inside the powder layers [1], squeezed voids between layers [4], and surface roughness. When the liquid viscosity is high, warp of the parts will occur due to overheating, especially on the first few layers. This is because the internal stresses are caused by the large temperature gradient between the part and the platform. The warp of SLM parts will lead to cracks between adjacent lines or delamination between neighboring layers [5]. In addition, cracks or delamination will also happen since higher cooling speed results in more formation of the brittle martensitic phase [6]. Both balling and overheating phenomena lead to building failure about the part density, mechanical properties, and dimensional accuracy during the SLM process, so detecting balling and overheating phenomena is the primary task in the monitoring.

Many attempts have been studied to correlate the process measurements to the part quality [7]. The SLM process is a

✉ Jerry Ying Hsi Fuh
jerry.fuh@nus.edu.sg

[1] Department of Automation, University of Science and Technology of China, Hefei 230026, China

[2] Department of Mechanical Engineering, National University of Singapore, Singapore 117575, Singapore

[3] Institute of Advanced Manufacturing Technology, Chinese Academy of Science, Changzhou 213164, China

non-stationary thermal process accompanied by optical, acoustic, electron, and other signals. Various process monitoring techniques have been implemented for detecting the melted sates from the SLM process. Kruth et al. developed a series of monitoring and control approaches for melting pool using combined cameras and photo diodes on the SLM system [8, 9]. Off-line experiments illustrated that there was a good correspondence between the in situ monitoring result and the actual quality in the products. The results indicated that the pores in the parts could be linked to melting pool variations. Lane et al. [10] conducted multiple sensor detections on a commercial LPBF machine during fabrication of a nickel alloy 625 AM part. Synchronized data was obtained by measuring a building part with an overhang structure. Residual heat and cooling rates were observed using thermal and visible cameras. Additionally, there appeared a relationship between frequency of photo detector signal and melt pool motion. Rieder et al. [11] demonstrated an online monitoring system using ultrasonic to inspect the built-up components. The captured signals offered inferred information for qualitative evaluation of residual stresses and porosity within finished parts. Kanko et al. [12] developed a morphology-based defect detection approach through an inline coherent imaging setup to monitor the melt pool morphology variations coaxially. The result showed that the melt pool fluctuations strongly influenced the final track quality and process defects resulting from poor parameter regimes.

All the monitoring methods above are either using coaxial setups or using off-axial monitoring setups. Using coaxial setups, the laser could be affected by the lens characteristics in a Lagrangian reference frame. Using off-axial monitoring setups, the laser is easily affected by issues such as the clamping position, angle, and distance even though the setup receives intense signals in a Eulerian reference frame. Acoustic sensors have many advantages in the monitoring of the SLM process since they are non-contact, non-destructive, and flexible. Setups using acoustic sensors have been widely used in laser welding processes, in which acoustic signals were used to identify the keyhole, no-keyhole, and cutting models successfully [13, 14]. However, acoustic signals have not been successfully used for the SLM process monitoring yet. The melting process of the SLM is inside a sealed chamber, so the environment noise is relatively stable compared to welding processes. Therefore, it is workable for using acoustic signals to monitor the SLM process. To overcome this problem, Ye et al. [15] applied a microphone to collect the acoustic signal for monitoring the characteristics during the SLM process. The forming mechanism of acoustic signal was investigated, and a good mapping between acoustic signals and laser power or laser scanning speed was found during the SLM process.

For the current methods, such as [9–12, 15], the monitoring methods mostly focused on the experimental setup and variable measurement, but fewer studies conducted the intelligent process monitoring and defect detection. Quicker speed, higher recognition accuracy, and fewer computation amounts are required in the in situ monitoring process. Hence, a proper intelligent recognition method is required to monitor the track formation during the SLM process. Intelligent methods have been widely applied in manufacturing process monitoring and defect detection. Among them, neural networks (NN) are the most studied method [16] and have been utilized for the IC engine fault detection [17], machine tool wear classification [18], welding defect recognition [19], and gearbox bearing fault detection [20]. Another effective and efficient intelligent method is support vector machine (SVM), with applications in rotating machinery component fault diagnosis [21] and tool condition monitoring for milling process [22]. All these intelligent methods above must make data preprocessing, denoising, and feature extraction, introducing many sequential steps. The sequential steps are accompanied with complex structures and low processing speed, and it is inconvenient in the in situ SLM process monitoring and defect diagnosis. Hence, a simplified monitoring framework is necessary. The lately developed deep belief networks (DBN) [23] could meet this need. In the DBN, it is performed to design features with generative pre-training and slightly adjust the features with discriminative fine tuning to achieve better recognition from raw signals. The DBN method has been recently applied for acoustic recognition due to the powerful learning capability of the higher-order topological features and good discrimination between classes of interest [24, 25]. However, the promising DBN method has yet to be employed for the monitoring and defect diagnosis of SLM process.

In this paper, the DBN is put forward to monitor the quality of the components using original acoustic signals from the SLM process. In Section 2, it is clarified the rationale and feasibility of defect detection by DBN using acoustic signals in the SLM processing. In Section 3, experimental setup is designed to verify the proposed monitoring method. In addition, results from multilayer perceptron (MLP) and SVM methods are used to compare with that from DBN in the diagnosis recognition. The conclusions in Section 4 are provided for the monitoring of SLM process.

2 SLM monitoring and defect detection with DBN using acoustic signals

2.1 The rationale of monitoring SLM process with acoustic signals

During the SLM processing, there exist melting pool, plasma, and spatter. Plasma is generated by laser energy irradiating the vaporization from the process, which changes with the laser energy density. The fluctuation of plasma during laser processing can strongly change the propagation of radiation by

reflection or refraction [26]. Underheating or overheating over metal powder by laser processing is accompanied with dynamic variation of plasma. The plasma density N_P goes up with ion density N and vapor density N_M as surface temperature T increases.

$$N_p = 3N_M d\Delta N \exp(-(E-\varphi)/kT) \quad (1)$$

where d is the laser radiation focal spot diameter, Δ is the cross section for atoms, E is the ionization potential of an atom, φ is the work function of a metal Δ, and k submits to the expression $kd = \pi/2$. As the increasing plasma adds the plasma density N_P, the atmosphere pressure P, which determines the intensity of the acoustic signal, fluctuates surrounding the melt pool. The acoustic intensity I can be formulated as

$$I = \frac{P^2}{f(\mathrm{N}_P)v} \quad (2)$$

where the air density $f(\mathrm{N}_P)$ is a function of plasma density and v is the sound speed. The air density, which is collected by the microphone near the melting site, is determined by the dynamics of the plasma density N_P. The behavior of laser processing in the SLM technology is connected with the variation of the plasma. Therefore, acoustic signals have relationships with the track formation during the SLM process.

2.2 The signal properties of acoustic signals

Figures 1 and 2 show acoustic signals with melting and without melting in time and frequency domains separately. Signals from without melting process were collected when the laser was on but not melting the powder. In the time domain as illustrated in Fig. 1, the amplitude with melting, which changes during the formation transforming, is much larger than that without melting. In the frequency domain of Fig. 2, there exists a narrow frequency range, after which the signals can be removed as noise. For the narrow frequency range, signal-to-noise ratio (SNR) was fixed at 10 dB. We use f_A to represent the mean frequency of this transitional area, as highlighted in Fig. 2. It is noted that f_A largely depends on the formation during the SLM process. Additionally, the numbers, size, and location of the amplitude summits in the frequency domain are various as the track formations change.

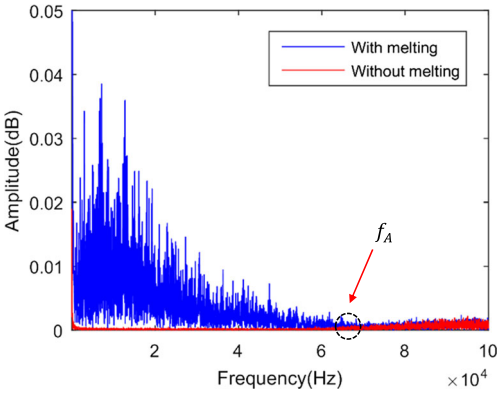

Fig. 2 Acoustic signals with melting and without melting in the frequency domain, where acoustic signals with melting were at scanning speed 100 mm/s, layer thickness 50 μm, and laser power 100 W

In order to analyze the characteristics of the acoustic signal, acoustic signals were converted into frequency domain by power spectral density (PSD) as shown in Fig. 3. Red line represents pure noise, which is collected without melting. The noise is mainly from the machine operating, environment noise, and their harmonic response, which is mostly among the low frequency range. Acoustic signals with melting determine a wide frequency range (0~65 kHz for the case in Fig. 2). In the following Section 3.2.1, it will perform the specific analysis for the low frequency from 0 to 3000 Hz between acoustic signals with melting and without melting.

Figure 4 indicates the different phenomena of balling and cracks after various melting conditions, which produce acoustic signals with distinct properties. Molten states are relative to the energy density E input into the powder, which is

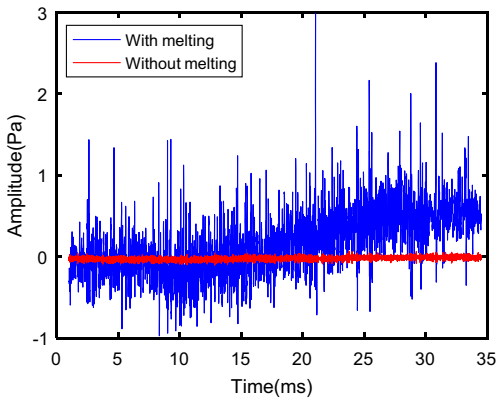

Fig. 1 Acoustic signals with melting and without melting in the time domain, where acoustic signals with melting were at scanning speed 100 mm/s, layer thickness 50 μm, and laser power 100 W

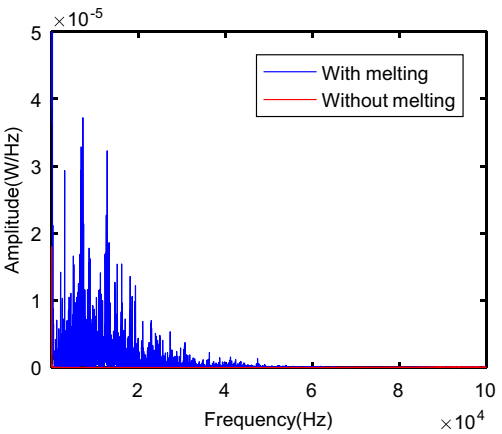

Fig. 3 Acoustic signals with melting and without melting after PSD

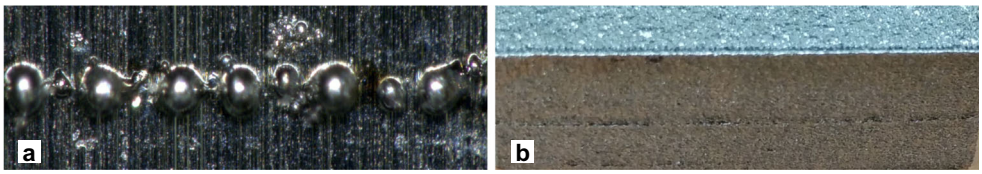

Fig. 4 Balling (**a**) and crack (**b**) appearance after SLM process

contributed by the scanning speed S, laser diameter D, hatch distance H, layer thickness T, and laser power P, defined as follows

$$E = \frac{P}{S \times H \times T \times D} \tag{3}$$

The melted states are determined by the laser energy density to a degree. Nevertheless, when there are multiple variables changing, the melted states are also affected by other factors such as the powder mass moving under the laser. Hence, process monitoring for the SLM is more necessary.

In Fig. 4a, balls appear at the surface of the work piece, which will result in building failure in squeezed voids, pores, and surface roughness in a part. As shown in Fig. 4b, cracks and delamination happen between layers in the part. All the serious problems in Fig. 4 result from balling or overheating. The formation of balling, slight balling, overheating, slight overheating, and normal phenomena will be distinguished by the DBN algorithm in the following.

2.3 Defect diagnosis using the DBN

Deep learning is a set of machine learning algorithms that model high-level abstractions of input data by using complex model architectures, mainly based on multiple layers of nonlinear transformations [23, 24]. Introduced by Hinton et al. [23], the DBN is a probabilistic graphical model that contains numerous layers for deep learning. Every layer progressively captures more composite patterns of data for dimension reduction, pattern analysis, and classification [27]. During the past several years, the DBN has made important influences on a wide range of applications, especially in acoustic molding and analysis. For instance, there are sound quality prediction [28], speech synthesis [29], and audio feature extraction as well as recognition [24, 25]. The key feature of the DBN learning algorithm is its layer-by-layer training, which can be repeated several times to learn a deep, hierarchical probabilistic model efficiently. DBN learning algorithm is composed of a stack of restricted Boltzmann machines (RBMs). An RBM is a network with symmetrically coupled stochastic binary units. It is determined by a set of visible units $v \in [0, 1]$, hidden units $h \in [0, 1]$, and connections between the visible and hidden neurons. The hierarchical structure of the DBN contains a single visible layer $\mathbf{v}$ and L hidden layers $\mathbf{h}^1, \ldots, \mathbf{h}^l, \ldots, \mathbf{h}^L$.

A DBN structure makes effective use of unlabeled data, interpreting a probabilistic generative model, and alleviating the problem of overfitting. The strategy of layer-wise unsupervised training followed by supervised fine-tuning allows efficient training of deep networks. Pre-training based on the stacked-up RBMs has been found to work well regardless of a large or small amount of training data [30]. The energy function of a joint configuration, which determines the probability distribution by the weights of connections, the biases of visible units, and the biases of hidden units in a binary RBM of the l_{th} level, is defined as

$$E(\mathbf{v}, \mathbf{h}) = -\sum_{i=1}^{n} a_i v_i - \sum_{j=1}^{m} b_j h_j - \sum_{i=1}^{n} \sum_{j=1}^{m} v_i h_j w_{ij} \tag{4}$$

where w_{ij} is the symmetric interaction term between the visible unit i and hidden units j, a_i, and b_j represent bias terms for visible units and hidden units respectively. The variable set $\theta = (\mathbf{w}, \mathbf{a}, \mathbf{b})$ is parameters to determine the RBM model, and the target of RBM training is to find the optimum θ^* that represents the training samples.

The joint probability distribution for visible and hidden units is defined as

$$p(\mathbf{v}, \mathbf{h}) = \frac{e^{-E(\mathbf{v},\mathbf{h})}}{Z} \tag{5}$$

where

$$Z = \sum_{\mathbf{v},\mathbf{h}} e^{-E(\mathbf{v},\mathbf{h})} \tag{6}$$

is a normalizing factor or a partition function, and it is obtained by summing over all the possible pairs of visible and hidden vectors. Similarly, the probability that the network assigns to a visible vector $\mathbf{v}$ is given by summing over all possible hidden vectors

$$p(\mathbf{v}) = \frac{\sum_{\mathbf{h}} e^{-E(\mathbf{v},\mathbf{h})}}{Z} \tag{7}$$

The probability that the network assigns to a visible vector will be increased by adjusting the weights and biases to decrease the energy of that vector, and contributes more to the partition function. It can be updated by taking the derivative of the log probability with respect to the weight

$$\frac{\partial \log p(\mathbf{v})}{\partial w_{ij}} = \langle v_i h_j \rangle_{data} - \langle v_i h_j \rangle_{model} \tag{8}$$

where the angle brackets are used to denote expectations specified. As a result, a simple learning rule for performing stochastic steepest ascent can be obtained

$$\Delta w_{ij} = \varepsilon\left(\langle v_i h_j\rangle_{data} - \langle v_i h_j\rangle_{model}\right) \tag{9}$$

where ε is a learning rate.

As there are no direct connections between hidden units in an RBM, it is convenient to get an unbiased sample of $\langle v_i h_j\rangle_{data}$. Given a randomly selected visible vector **v**, the binary state of the hidden unit h_j is set to 1 with probability

$$p(h_j = 1|\mathbf{v}) = g\left(b_j + \sum_i v_i w_{ij}\right) \tag{10}$$

where $g(z) = 1/(1 + \exp(-z))$ is the logistic sigmoid function. The $v_i h_j$ is then an unbiased sample. Similarly, it is defined an unbiased sample to the visible unit state under a given hidden vector as

$$p(v_i = 1|\mathbf{h}) = g\left(a_i + \sum_j h_j w_{ij}\right) \tag{11}$$

To get an unbiased sample of $\langle v_i h_j\rangle_{model}$, a faster learning procedure was proposed in [30]. This starts by setting the visible unit states as a training vector. Then, using Eq. (10), the hidden binary states are all computed in parallel. Once binary states were chosen for the hidden units, with a probability given by Eq. (11), a reconstruction model is produced by setting each v_i to 1. The increment of weight is then given by

$$\Delta w_{ij} = \varepsilon\left(\langle v_i h_j\rangle_{data} - \langle v_i h_j\rangle_{recon}\right) \tag{12}$$

For the biases, it uses the same learning rule that uses the states of individual units rather than pairwise products. The DBN structure and model parameters $\theta = (\mathbf{w}, \mathbf{a}, \mathbf{b})$ are finally trained and updated according to the following learning rules:

$$w_{ij} = \eta w_{ij} + \varepsilon\left(\langle v_i h_j\rangle_{data} - \langle v_i h_j\rangle_{recon}\right) \tag{13a}$$

$$a_i = a_i + \varepsilon\left(\langle v_i\rangle_{data} - \langle v_i\rangle_{model}\right) \tag{13b}$$

$$b_j = b_j + \varepsilon\left(\langle h_j\rangle_{data} - \langle h_j\rangle_{model}\right) \tag{13c}$$

where the η is the regularization term for the weight.

Figure 5 shows the architecture of the DBN for defect recognition with the visible unit v_i of acoustic signals from the SLM process. The network consists of three hidden layers, and the pre-training procedure consists of three stages of unsupervised learning. During the final fine-tuning with back propagation (BP), all the parameters are trained via a supervised learning rule using initial values obtained from the pre-training.

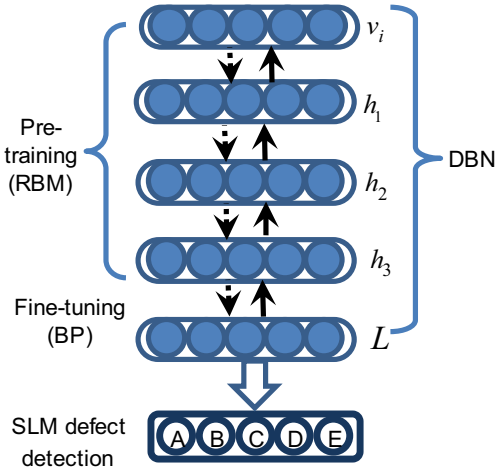

Fig. 5 An illustration of DBN with stacked RBMs for five-state recognition in the SLM process

3 Experiments, results, and discussions

3.1 Experimental design

As shown in Fig. 6, the experimental monitoring system consists of an own custom-designed SLM system and an acoustic signal acquisition system. This SLM system is composed by a laser, a powder-spreading device, and a controller panel. The controller panel can adjust the process parameters by connecting to the powder-spreading device, laser power, and gas cylinder. The acoustic signal acquisition system includes a 3780C1 PCB microphone fixed at an angle of 30° over the platform and a SIRUSm data acquisition system as depicted in Fig. 7. It has the frequency response from 0 Hz to 100 kHz. A series of SLM experiments is conducted on the 304 stainless steel powders with a modulated pulse laser. To easily ensure the formation of each track line, the hatch distances are large up to 1.5 mm to eliminate the thermal effect between adjacent lines. According to the relationships among acoustic signals, energy densities, and the track formation, energy densities into the powder are changed to obtain the melted states of overheating, slight overheating, normal, slight balling, and balling as listed

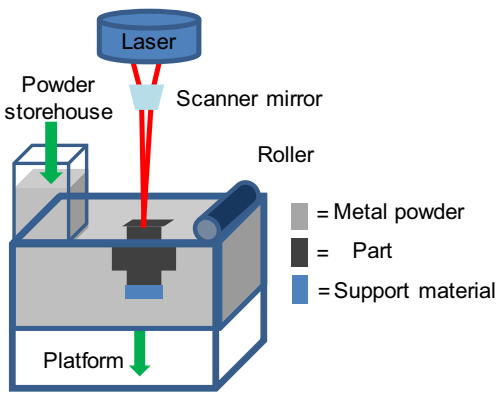

Fig. 6 Schematic depicting the metal SLM process technology

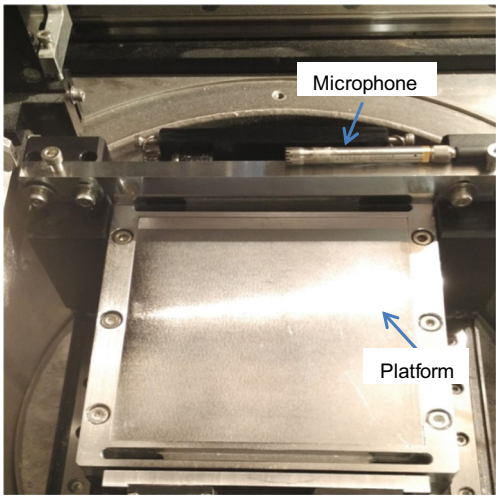

Fig. 7 Experiment setups with an acoustic signal acquisition system

in Table 1. The parameters are changing from scanning speeds of 600, 100, and 50 mm/s at laser power of 100 W to laser power of 60 and 160 W at scanning speeds of 100 mm/s.

With the experimental configuration, varied parameters were applied to obtain five different patterns. For each pattern, 10-mm lines at various conditions are repeated with 200 kHz sampling frequency of the acoustic acquisition system to obtain 3860 sets of balling, 4302 sets of slight balling, 5489 sets of normal, 4776 sets of slight overheating, and 4321 sets of overheating signals. In this experiment, different energy densities were input into the same 50-um-thickness powder layers at the same hatch distance with laser radiation focal spot diameter 100 μm. Distinctive phenomena of class A, class B, class C, class D, and class E were generated from different laser energy densities. They are slight balling, balling, normal, overheating, and slight overheating separated by the formation phenomena and widths as demonstrated in Fig. 8.

3.2 Results and discussion

3.2.1 Defect pattern features and signal preprocessing

For the experimental observations of Fig. 8, the laser energy density of class B is smaller than that of class A, while the melted state is smoother. This is because the mass of the powder moving into the melt pool decreases with the high scanning speed increase. The phenomena were also shown in [31] at the same laser energies with different scanning speed and laser power. Therefore, laser energy density is just an indication of the energy input when a single melting parameter changes. The balling degree of classes A and B and their wettability are apparent as depicted in Fig. 8. For class C, the wettability is good and there are small balls generated from powder spatter that can be melted by the adjacent remelting. Large balls attached to the track surface appear in class D and class E since more energy input induces more liquid spatters falling back onto the melting sites. Recoil pressure on the melting pool rises with the energy input growth so the number and the size of balls attached to the track surface increase from overheating class D to class E.

Besides the acoustic signals corresponding to class C as demonstrated in Fig. 1, the signals in time domain corresponding to the other four classes are shown in Fig. 9. The signals are much more overlapped, which cannot be classified by a simple algorithm. The frequency below f_A dominates most features and energy as shown in Fig. 3; thus, low frequency from 0 to 3000 Hz was zoomed in for specific analysis as shown in Fig. 10. Comparing acoustic signals with melting and without melting after PSD, the peaks before 500 Hz were basic noise amplified by resonated signals. The next peak at 1160 Hz was the resonance frequency from metal powder processing by laser. Therefore, the sample window size of acoustic signals (time domain) $x(t)$ was 200 for a set depending on the frequency resolution and time resolution of the acoustic signal. From this way, signals from five patterns of normal, balling, slight balling, slight overheating, and overheating were collected experimentally. Standardization was used to make the collected data into normalization with zero mean and unit variance, and therefore, all parameters had the same scale for a fair comparison between them, avoiding performance of inaccuracy and extensive data redundancy. The location of frequency f_A varied with the track formations changing. Noise is distributed among all the frequency bands (Fig. 2), but within the high frequency range, the energy of noise was close to that of melting signals as depicted in Fig. 3. Denoising was performed with a butter frequency band pass filter from 500 to 90,000 Hz.

Table 1 Condition patterns of the melting results with various melting parameters

Defect class	Defect pattern	Hatch distance (mm)	Layer thickness (μm)	Laser diameter (μm)	Scanning speed (mm/s)	Laser power (W)
Class A	Balling	1.5	50	100	100	60
Class B	Slight balling	1.5	50	100	600	100
Class C	Normal	1.5	50	100	100	100
Class D	Slight overheating	1.5	50	100	100	160
Class E	Overheating	1.5	50	100	50	100

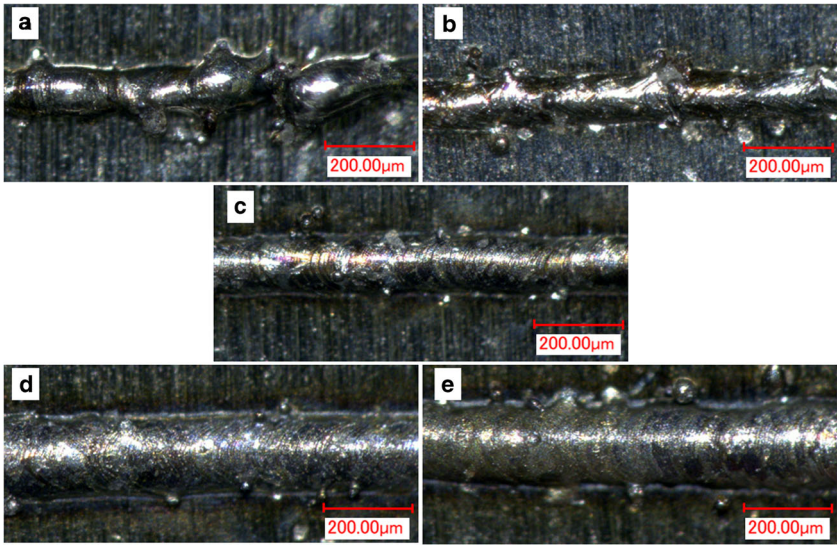

Fig. 8 Defect states of the SLM process, in which **a**, **b**, **c**, **d**, and **e** are balling, slight balling, normal, slight overheating, and overheating

3.2.2 DBN training and classification performance

1. The DBN training

According to the DBN modeling approaches in Section 2.3, the DBN is trained in the following procedure:

(a) Train the first layer as an RBM that models the raw (frequency domain) input $\mathbf{v} = x(f)$ as its visible layer.

(b) Use that first layer to obtain a representation of the input that will be used as data for the second layer. It can be chosen as being the mean activations $p(\mathbf{h}^1 = 1 | \mathbf{v})$.

(c) Train the second layer as an RBM, taking the transformed data as the visible layer of that RBM.

(d) Iterate (b) and (c) for the desired number of layers, each time propagating upward either samples or mean values.

(e) Fine-tune all the parameters of this deep architecture with respect to the learning criterion Eq. (13).

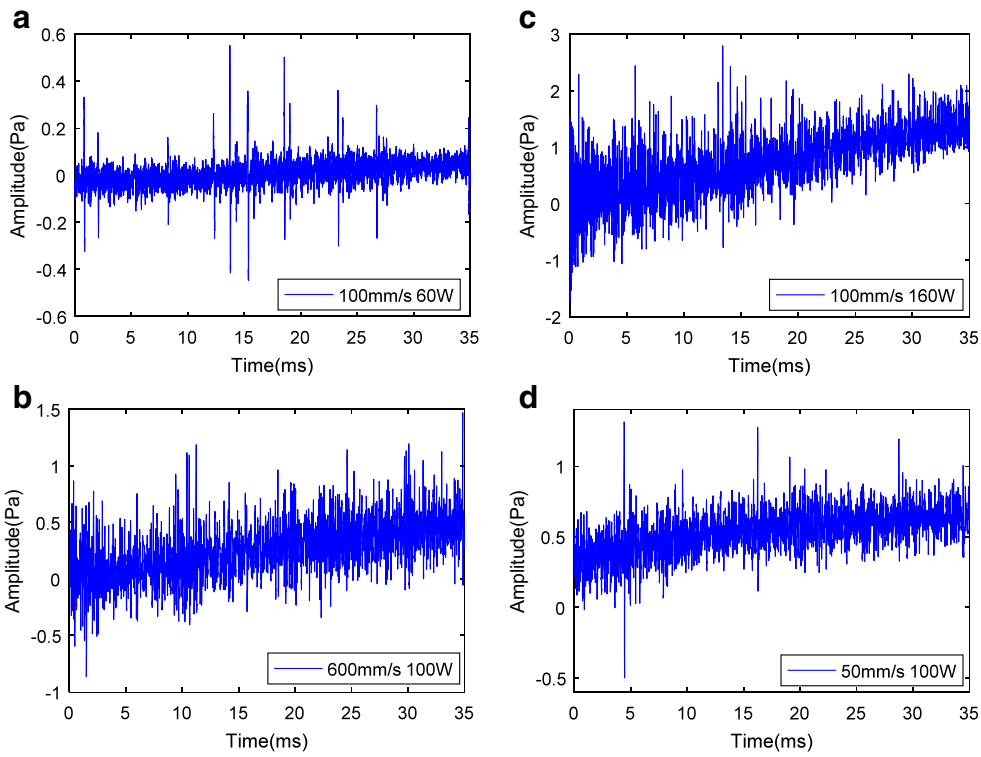

Fig. 9 Acoustic signals in the time domain, which are corresponding to classes A, B, D, and E

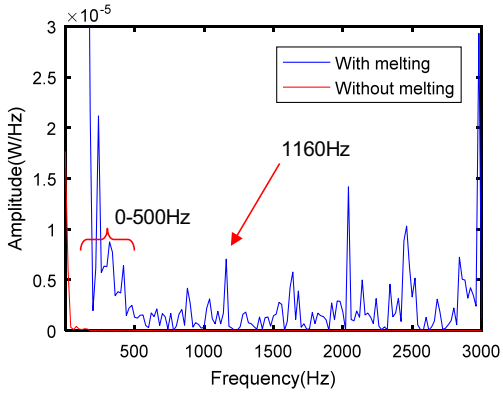

Fig. 10 Acoustic signals with melting and without melting after PSD from 0 to 3 kHz

The classification with a DBN model was designed with four-level RBMs. The model parameters were as follows: the numbers to the units in all hidden layers of DBN were 300 and the number of units in the fourth output layer was also 300. Classification procedure was produced by a 300-300-300-300 DBN mapping the data input. Numbers of pre-training epochs of DBN were all 20 with an unsupervised learning rate of 0.001 and 100 batch size, and the number of fine-tuning epochs of DBN was 200 with a supervised learning rate of 0.01 and 100 batch size as illustrated in Fig. 11.

2. Classification performances

With the deep presentation in the multiple RBMs, a softmax layer [30] at the top is used to diagnose the defects from the free energies of all the class-specific RBMs. Specifically, the log probability that the RBM trained on class c assigns to the test vector $\mathbf{t}$ is given in the softmax layer

$$\log P(class = c|\mathbf{t}) = \frac{e^{-E_c(\mathbf{t})-\log Z_c}}{\sum_d e^{-E_c(\mathbf{t})-\log Z_d}} \quad (14)$$

where Z_c is the partition function of the corresponding RBM.

The 60% of total samples for training and 40% for testing and validation were randomly separated before recognition processing. They were acoustic signals of different track formations, which were preprocessed by the original, the FFT, and the FFT with denoising separately. The DBN structure with larger numbers of RBM units as well as hidden layers would lead to over fitting and huge computation burden, but the structure with few numbers of them could not learn the signal information to make an effective model as shown in Fig. 12. Cross-validation was performed to evaluate the recognition model with no over fitting when the model was established. After five times repeated cross-validation procedures, five results were again averaged to produce a single classification rate. The average classification rates out of five repeated DBN structure runs for the diagnosis approach were 72.43% with the original data, 95.93% with the data after FFT, and 95.87% with the data after FFT and denoising. There was a little decline when introducing a band pass filter since a band pass filter cut off information within the removed frequency band.

3.2.3 Comparison with other related methods

Due to their close relation to the DBN and the populations in defect detections, MLP and SVM recognition methods were implemented for a comparison of the results. In the MLP model, a three-layer feed-forward network with 10 neurons in the hidden layer was created. As a similar method to the DBN, MLP had connections with the previous layer. The first layer had a connection from the network input, and the final layer produced the network's output. There was no feedback between layers. Table 2 represents the averaged results of five repeated runs of diagnosis with MLP. They are 46.07% with the original data, 82.34% with the data after FFT, and 82.40% with the data after FFT and denoising. The variation of the five repeated results from MLP was larger than those from DBN and SVM because there was no feature extraction before MLP

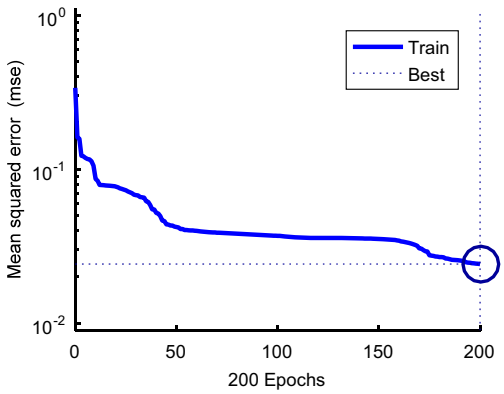

Fig. 11 Performance of the fine-tuning with 200 epochs in the DBN training with data after FFT. Best training performance is 0.024249 at epoch 200

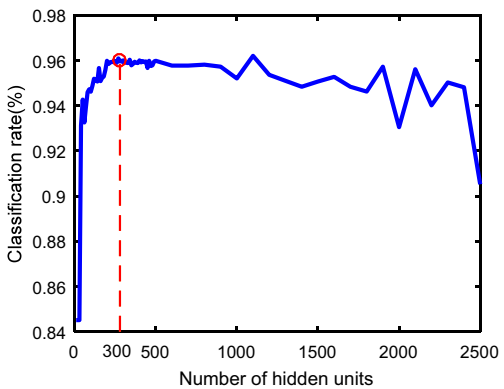

Fig. 12 Classification rate from the DBN recognition method with various numbers of hidden units with data after FFT. The classification rate is 96.03% at 300 hidden units for one run

training, and the samples were not enough to model the fitting function.

All the sampling acoustic signals x were set as signal features, and the number of feature was large compared with the samples. Therefore, linear kernel function was used in the training of the SVM model. The classification rate and efficiency of the diagnosis techniques were tested and validated with the testing and validation datasets using the trained defect diagnosis SVM model. The average classification rates out of five repeated runs for the SVM diagnosis approach were 67.82% with the original data, 97.86% with the data after FFT, and 98.01% with the data after FFT and denoising.

In all of three recognition methods, there was a little change between the diagnosis using FFT combining denoising data and that using FFT data. The weights of the same noise among each feature became small when the recognition structures were trained, so there was little influence on the classification results. Therefore, the noise inside weakly affected the defect diagnosis accuracy.

From the results presented in Table 2, DBN method provided the best classification rate of 72.43% in various defects with the raw data. The results from the DBN method improved 23.50% as the FFT was added, while those from MLP and SVM increased 36.27 and 30.04%. The result growth of the SVM and MLP methods was bigger than that of the DBN. This was because the DBN had learnt features from the raw data itself, and data processing played a small role in the recognition process. Moreover, DBN could greedily pre-train the initial data to obtain high-order information by stacking RBMs before finally using the proposed algorithm to tune the generative model actually, while the neural network MLP just simply mapped the initial data to approximating functions with multilayer perceptrons directly. Hence, the deviation values between the DBN and the MLP decreased from 26.36 to 13.59% as the FFT procedure was added. In addition, the classification results from the DBN and MLP models become closer when more data preprocessing was increased.

For the comparison between SVM and DBN, the result of SVM was a little better than that of DBN when adding data preprocessing inside, while it was poor for the raw data without any data processing. SVM outperformed other methods in pattern classification when there are balanced data set and noise free or little since it is based on the statistical learning theory. However, SVM cannot explicitly present the relationships learned from data.

For these reasons above, the DBN constructs a deep architecture to learn deep features of the input data and capture the correlation between features to obtain the high-level information. Furthermore, it reduces the complexity and selects the primary information of the input data. High-level learning by the generative model is superior for discriminating the track formations of interest when there is less preprocessing input. As a result of this, DBNs can make the real-time monitoring of the SLM process possible without any data preprocessing using acoustic signals.

3.2.4 Generalization of the DBN

To show the generalization of the DBN structure to the SLM process monitoring, more experiments 1, 2, 3, 4, and 5 were added to the tests and validated the model. In these tests, there are no identical melted states but states with similar trends since the melted states vary at the same energy density of different scanning speed and laser power as depicted in Section 3.1. Experiments 1, 2, 3, 4, and 5 with random parameter combinations were employed for testing and validating. There were uniformities within the balling, normal, and overheating acoustic signals respectively so the states could be classified into the closest ones. As shown in Table 3, the classification rate 70.57% was obtained from the DBN model using raw data. Differences of the classification rates between using raw data and using other preprocessing methods decreased to 22.43 and 23.06% separately. Classification rate from data after FFT and denoising was slightly better than that

Table 2 Comparison without and with data preprocessing

Peered method	Data processing	Classification rate (%)	Difference (1) (%)	Difference (2) (%)
DBN	Raw data	*72.43*		
	Data after FFT	95.93	23.50	
	Data after FFT and denoising	95.87	23.44	
MLP	Raw data	*46.07*		26.36
	Data after FFT	82.34	36.27	13.59
	Data after FFT and denoising	82.40	36.33	13.47
SVM	Raw data	*67.82*		4.61
	Data after FFT	97.86	30.04	− 1.93
	Data after FFT and denoising	98.01	30.19	− 2.14

Difference (1) is the classification rate difference between raw data and data with preprocessing. Difference (2) is the classification rate difference between the DBN and peered methods

Table 3 Test and validation with other samples

Experiments	Defect pattern	Scanning speed (mm/s)	Laser power (W)	Classification rate (%)		
				Raw data	Data after FFT	Data after FFT and denoising
1	Balling	100	50	70.57	93.00	93.63
2	Slight balling	700	100			
3	Normal	110	100			
4	Slight overheating	100	150			
5	Overheating	40	100			
Difference (1)					22.43	23.06

from data after FFT. This illustrates that f_A moves with the formation changing during the SLM process as shown in Section 2.2. The DBN model without data preprocessing performs more superior in recognition during the SLM process.

4 Conclusions

In this paper, acoustic signals were proposed to detect the defects by the DBN method during the SLM process. Acoustic signals have relationships with the track formation during the SLM process since the formation and acoustic signals are both connected with the plasma variation. The acoustic method detected the defect with less data collected from a flexible setup. Acoustic signals were gathered from five defect patterns and used for defect identification by the DBN method. The DBN method extracted the high hierarchical information and relationship from the raw acoustic signals, which avoided feature extractions and data preprocessing. It performed superior compared with the utilities of SVM and MLP intelligent methods, and there was a generalization among the defect patterns from experiments with random parameter combinations. Hence, this research provides a convenient and possible solution to realize the process monitoring and defect detection during the SLM process.

References

1. Attar H, Calin M, Zhang L, Scudino S, Eckert J (2014) Manufacture by selective laser melting and mechanical behavior of commercially pure titanium. Mater Sci Eng 593:170–177
2. Malekipour E, El-Mounayri H (2017) Common defects and contributing parameters in powder bed fusion AM process and their classification for online monitoring and control: a review. Int J Adv Manuf Tech, Accepted
3. Agarwala M, Bourell D, Beaman J, Marcus H, Barlow J (1995) Direct selective laser sintering of metals. Rapid Prototyping J 1(1):26–36
4. Thijs L, Verhaeghe F, Craeghs T, Van Humbeeck J, Kruth JP (2010) A study of the microstructural evolution during selective laser melting of Ti–6Al–4V. Acta Mater 58(9):3303–3312
5. Ramakrishnan P (2002) Residual stresses in powder-metal processing. In: Handbook of residual stresses and deformation of steel. Ohio: ASM International, Materials Park, pp 397–423
6. Kempen K, Vrancken B, Buls S, Thijs L, Humbeeck JV, Kruth JP (2014) Selective laser melting of crack-free high density M2 high speed steel parts by baseplate preheating. J Manuf Sci Eng 136(6): 061026
7. Tapia G, Elwany A (2014) A review on process monitoring and control in metal-based additive manufacturing. J Manuf Sci Eng 136(6):060801
8. Craeghs T, Clijsters S, Yasa E, Kruth JP Online quality control of selective laser melting. In: Proceedings of the Solid Freeform Fabrication Symposium, 2011. University of Texas at Austin, pp 212–226
9. Kruth JP, Levy G, Klocke F, Childs THC (2007) Consolidation phenomena in laser and powder-bed based layered manufacturing. CIRP Ann 56(2):730–759
10. Lane B, Whitenton E, Moylan S (2016) Multiple sensor detection of process phenomena in laser powder bed fusion. In: International Society for Optics and Photonics, pp 9861041–9861049
11. Rieder H, Dillhöfer A, Spies M, Bamberg J, Hess T (2014) Online monitoring of additive manufacturing processes using ultrasound. In: Proceedings of the 11th European Conference on Non-Destructive Testing. pp 6–10
12. Kanko JA, Sibley AP, Fraser JM (2016) In situ morphology-based defect detection of selective laser melting through inline coherent imaging. J Mater Process Technol 231:488–500
13. Song S, Chen H, Lin T, Wu D, Chen S (2016) Penetration state recognition based on the double-sound-sources characteristic of VPPAW and hidden Markov model. J Mater Process Technol 234: 33–44
14. Saad E, Wang H, Kovacevic R (2006) Classification of molten pool modes in variable polarity plasma arc welding based on acoustic signature. J Mater Process Technol 174(1):127–136
15. Ye D, Zhang Y, Zhu K, Hong G, YingHsi J (2017) Characterization of acoustic signals during a direct metal laser sintering process. In: Advances in energy science and equipment engineering II. CRC Press, pp 1315–1320
16. Wang F, Devabhaktuni VK, Xi C, Zhang QJ (1999) Neural network structures and training algorithms for RF and microwave applications. Int J Rf Microw C E 9(3):216–240
17. Chen J, Randall RB, Peeters B (2016) Advanced diagnostic system for piston slap faults in IC engines, based on the non-stationary characteristics of the vibration signals. Mech Syst Signal Process 75:434–454

18. Saglam H (2011) Tool wear monitoring in bandsawing using neural networks and Taguchi's design of experiments. Int J Adv Manuf Technol 55(9):969–982
19. Boaretto N, Centeno TM (2017) Automated detection of welding defects in pipelines from radiographic images DWDI. NDT E Int 86:7–13
20. Bangalore P, Tjernberg LB (2015) An artificial neural network approach for early fault detection of gearbox bearings. IEEE T Smart Grid 6(2):980–987
21. Saimurugan M, Ramachandran KI, Sugumaran V, Sakthivel NR (2011) Multi component fault diagnosis of rotational mechanical system based on decision tree and support vector machine. Expert Syst Appl 38(4):3819–3826
22. Lin X, Zhou B, Zhu L (2017) Sequential spindle current-based tool condition monitoring with support vector classifier for milling process. Int J Adv Manuf Technol 92(9):3319–3328
23. Roux NL, Bengio Y (2008) Representational power of restricted Boltzmann machines and deep belief networks. Neural Comput 20(6):1631–1649
24. Schmidt EM, Kim YE (2011) Learning emotion-based acoustic features with deep belief networks. In: Applications of Signal Processing to Audio and Acoustics (WASPAA), IEEE Workshop on, 2011. IEEE, pp 65–68
25. Huang HB, Li RX, Yang ML, Lim TC, Ding WP (2017) Evaluation of vehicle interior sound quality using a continuous restricted Boltzmann machine-based DBN. Mech Syst Signal Process 84: 245–267
26. Gladush GG, Smurov I (2011) Plasma phenomena in laser processing of materials. In: Physics of Laser Materials Processing Springer, pp 145–210
27. O'Connor P, Neil D, Liu S-C, Delbruck T, Pfeiffer M (2013) Real-time classification and sensor fusion with a spiking deep belief network. Front Neurosci 7
28. Huang HB, Huang XR, Li RX, Lim TC, Ding WP (2016) Sound quality prediction of vehicle interior noise using deep belief networks. Appl Acoust 113:149–161
29. Ling ZH, Deng L, Yu D (2013) Modeling spectral envelopes using restricted Boltzmann machines and deep belief networks for statistical parametric speech synthesis. IEEE T Audio Speech 21(10): 2129–2139
30. Salakhutdinov R, Hinton G (2009) Deep boltzmann machines. In: Artificial Intelligence and Statistics. pp 448–455
31. Li R, Liu J, Shi Y, Wang L, Jiang W (2012) Balling behavior of stainless steel and nickel powder during selective laser melting process. Int J Adv Manuf Technol 59(9):1025–1035